
Article:
Mamalis, D. orcid.org/0000-0002-3129-4270, Flanagan, T. and Ó Brádaigh, C.M. (2018) Effect of fibre straightness and sizing in carbon fibre reinforced powder epoxy composites. Composites Part A: Applied Science and Manufacturing, 110. pp. 93-105. ISSN 1359-835X

https://doi.org/10.1016/j.compositesa.2018.04.013

Effect of Fibre Straightness and Sizing in Carbon Fibre Reinforced Powder Epoxy Composites

Dimitrios Mamalis[#], Tomas Flanagan[*], Conchúr M. Ó Brádaigh[#]

[#]School of Engineering, Institute for Materials and Processes, The University of Edinburgh, Sanderson Building, Robert Stevenson Road, Edinburgh EH9 3FB, Scotland, United Kingdom

[*]ÉireComposites Teo., Indreabhán, Co. Galway, Ireland

Abstract

Carbon fibres with three different sizing agents were used to manufacture unidirectional composites based on powder epoxy resin. A specially designed tensioning apparatus was adopted to apply tension on fibres during the thermal curing cycle, in order to achieve an enhancement of fibre straightness. Chemical composition and surface morphologies of the carbon fibres were extensively characterised. The composites were evaluated using tensile, flexural and interlaminar shear strength tests, and mechanical performance measured based on fibre orientation, fracture modes and interfacial properties. The results demonstrated that composites processed with fibres under tension resulted in an increased unidirectional character in connection with the different amounts of sizing. Flexural and interlaminar testing of the laminates, in addition to Scanning Electron Microscopy and Dynamic Mechanical Thermal Analyses, revealed interfacial adhesion differences, emphasizing the importance of the adequate combination of the polymeric matrix and the type of reinforcement to the structural integrity of the composite.

1. Introduction

Epoxy resins (thermoset polymers) are of significant importance to the engineering field with fibre-reinforced epoxies being applied widely in the aeronautics, automotive, marine and renewable energy industries [1–7]. Epoxies are characterised by high stiffness, excellent chemical and corrosion resistance, high thermal and mechanical properties, exceptional adhesion to numerous substrates, low shrinkage during cure, outstanding electrical insulating properties, and the good processing ability under various conditions [4,8–11]. The extensive

use of epoxy thermosets in several high potential applications is restricted, however, by their inherent fracture toughness limitations, leading to brittleness, and delamination failures [8,12,13]. In the coating industry, powdered thermosets have been widely adopted, rather than conventional epoxy systems, due to the emission of zero, or near zero, volatile organic compounds (VOC), the absence of solvents, and the potential for extensive utilization as well as economical and environmentally friendly properties i.e. disposability and less hazardous wastes [14,15]. The most robust advantages of the powder epoxies are the characteristically low exothermic reaction during curing process compared to the conventional systems and the ability of the powder to melt, and flow, at elevated temperatures without significantly increasing the degree of cure [16,17]. Utilising the unique properties of the epoxy powders, improvements in the quality and uniformity of the cured material can be achieved with the use of powder epoxy resin, while also reducing the final production cost. These meaningful processing properties have attracted the interest of tidal and wind industries where the need of manufacturing thick-section composite structures is required e.g. turbine blades or root spars[18].

It is well-known that the fracture characteristics of carbon fibre reinforced polymers (CFRPs) are affected by a lot of factors including properties of raw materials, fibre content, orientation and straightness, voids, moisture, temperature and manufacturing processes. However, the ultimate performance of the composite is not only determined by the involved phases, but is also influenced to a large extent by the interphase formed between the two components [19–21]. Considering that the compatibility between the carbon fibres and resin matrix is one of the most fundamental parameters that controls effectively the properties of the composite, it is therefore necessary to research the interphase phenomena providing valuable insight for industry applications.

The interfacial bonding between the fibres and the polymer matrix is expected to be dependent on the surface properties of the fibre such as roughness, porosity and functional groups, on the chemical character of the matrix [19,22,23], on the presence of defects (voids, low cohesion) [19] and on residual thermal stresses [24]. The sizing materials (usually a thin polymeric coating applied on the surface of unsized carbon fibres [25,26] in low concentrations i.e. 0.3 – 1.5 wt.%, protect the brittle fibres from damage and improve the processability and structural integrity of the composite, alter the manner that the stress is transferred from the matrix to the fibres as well as promoting interface bonding performance [9,19,23]. In addition, the sizing agent can change the apparent surface energy of the carbon fibre, the wetting ability

and the physicochemical interactions with the epoxy matrices [27,28].

Manufacturing processes of FRPs involve the selection of appropriate materials, design ideas and fabrication techniques. Among the different fabrication processes, pultrusion is recognised as one of the most cost-effective and energy-efficient processes due to its high automation and great production rates [29–31]. The combination of pulling and extrusion methods adopted by this technique can deliver superior performance composites characterised by high fibre volumes as high as 70% and in turn enhancing the stiffness profile of the material [29]. Moreover, improvements in FRP properties have been found during pultrusion, as the fibres are pulled under tension in a continuous form resulting in exceptionally high straightness characteristics [29,32]. Recently, there is growing interest in the renewable energy industry for the use of pultruded sections or planks in the spar caps of very long (>60m) wind turbine blades, as well as for innovative vertical axis wind turbine blades (VAWT) [33,34].

The main aim of the present investigation is to gain a better understanding of the mechanical properties of powder-epoxy resin composites reinforced with UD carbon fibres for manufacturing out-of-autoclave components. The key challenge of the work was to demonstrate the effect of the type of sizing on the fibre surface, in conjunction with fibre straightness, on the mechanical performance of the laminates. A novel hand lay-up process was employed to manufacture powder-epoxy composites reinforced with three different types of carbon fibres. The fibre volume fraction, the void content and the fibre orientation of the composites were experimentally measured and compared to optical methods. Mechanical properties in terms of tensile, flexural, and interlaminar shear strength along with the optical characteristics of the tested/failed composite samples were evaluated. The understanding of the factors controlling and driving the dominant failure modes was an objective as well. Furthermore, the influence of fibre/matrix interphase on interfacial adhesion has been investigated through tensile, flexural properties and interlaminar strength connected with the carbon fibre surface roughness and sizing functional groups.

2. Experimental procedure

2.1 Materials and composite preparation

Commercially available continuous tow carbon fibres T700S-24K-50C (1% sizing agent), T700S-24K-F0E (0.7% sizing agent) and T700S-24K-60E (0.3% sizing agent) from TORAYCA® (Toray Industries, Inc.), were used in the present work. Powder epoxy resin (EC-CEP-0016) supplied from EireComposites Teo. with density 1.22 g/cm^3, was used as the matrix to manufacture the composite materials. The powder-epoxy used has recently been investigated by Maguire *et al.*, using characterisation techniques and a modelling methodology under various processing conditions, and proposed as a new high-quality, cost-effective alternative of manufacturing out-of-autoclave components for marine applications [16,35].

All initiators-reagents were mixed in the powder, the curing reaction was heat-activated and the supplier recommended a cure temperature at ~180ºC. Unidirectional carbon fibre powder epoxy composite (CFRP) plates with dimensions of 450 × 250 mm (length × width) and thicknesses of ~1 mm (5-plies) and ~3 mm (15-plies), were fabricated, respectively. Fig. 1(a) shows a representative image of the composite's lay-up i.e. the taped carbon fibres and the deposited powder epoxy (white material). Moreover, a novel hand lay-up process which used a specially designed tensioning apparatus was adopted such that the carbon fibres were kept in tension during the cure process, targeting an enhancement of fibre-straightness, see Fig. 1(b). Carbon fibre tows were cut to the desired length and laid side by side on a flat surface. The fibre tows were combed by hand to align any loose fibres and smooth the appearance of the tows. The taped fibres (plies) were loaded in the tensioning apparatus, Fig. 1(b), clamped at both ends and then tension of around 3000N was applied uniformly until fibres started sliding at both clamped ends. Note that the applied tension on the carbon fibre plies was estimated with two techniques by using a Newton-meter and a torque wrench. A mass of ~300Kg was applied uniformly on the fibre plies which was equalled to ~ 3000N according the Newton-meter readings. Also, a torque wrench was employed and the tightness of the screws that were helping to apply tension (extend the carbon fibres plies) was estimated. The measured value using the torque wrench revealed force values of the same order of magnitude as with the Newton-meter. However, this technique suffers from inaccuracy due to inconsistent or uncalibrated friction between the fasteners and used the screw-bar. The epoxy powder was distributed evenly on each ply aiming towards a 60:40 (carbon: epoxy) final weight ratio of the laminate. The thickness of a single ply was approximately 0.2 mm. Fig. 1(c) present a typical image of a final CF/epoxy composite laminate with thickness of 1mm (5 plies).

The thermal cycle applied to all the laminates (tensioned and non-tensioned) consisted of a drying stage; an isothermal dwell at 50±1 ºC for 400 min, B stage; isothermal dwell at ~120±1

ºC for 60 min and a curing cycle with a heating rate of 2±0.2 °C/min up to 180±1 °C, holding at this temperature at least 90 min, followed by cooling down to room temperature. The fabrication process was under vacuum conditions. All samples were consolidated by vacuum, and breather cloth was employed to remove the air bubbles and volatiles. The test coupons of all T700S/epoxy composite laminates were cut using a diamond saw (wet) technique to produce high quality smooth edges avoiding any defects/imperfections that might influence the final mechanical performance. Fibre volume fraction and void content of all the processed composites were determined by the acid digestion method according to ASTM D3171 (2009). Furthermore, neat epoxy plates were manufactured following the same thermal cycle as for the composites cases to provide a baseline for comparison. The neat resin was bagged and placed in the oven for drying, B-stage and cure cycle as described for the CFRP cases.

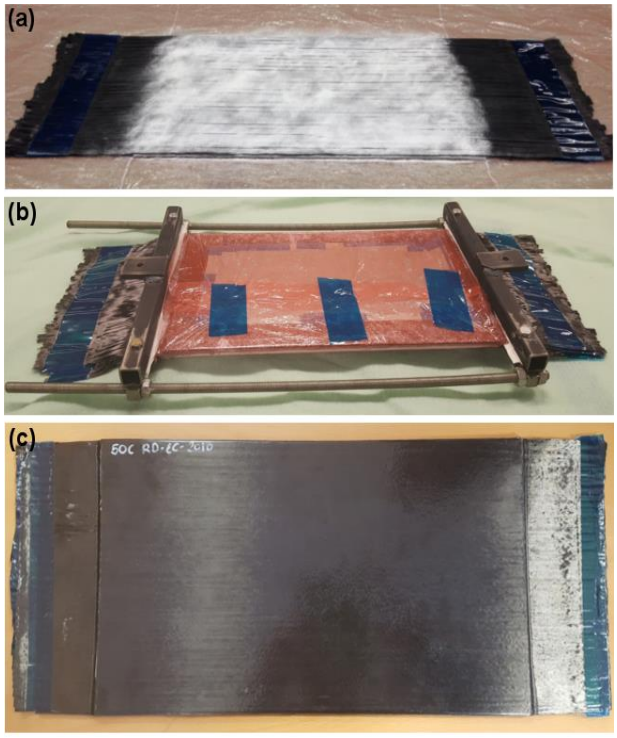

Fig. 1. Typical images of the (a) carbon fibre (black) powder epoxy (white) lay-up with no tension (b) apparatus used to apply tension on the fibres during the thermal cycle and (c) manufactured carbon fibre epoxy composite laminate.

2.2 Tensile Testing

Tensile tests were carried out in accordance with BS EN 2561 (1995) using a minimum of 15 specimens (dimensions: 250 length x 25 width x 1 mm thickness) for each composite family i.e. 50C, F0E and 60E. A minimum of 7 specimens were machined from each carbon fibre epoxy composite plate and subsequently tested. The composite specimens were prepared by bonding end-tabs of 1581 type glass-epoxy laminate, arranged at ± 45° (thickness between 0.5 mm and 1 mm) and bonded onto the specimen using an adhesive. The tensile tests for composites and polymer specimens were performed in a universal testing machine Zwick/Roell, model Z250, with hydraulic grips and MTS 632.85F-14 extensometer, at constant cross-speed between 2 and 5 mm/min. The calibration and verification of the measuring system i.e. 250 kN load cell, was based on ISO 7500-1 (2015) and ASTM E4 (2016) standards. The fitted extensometer was calibrated in accordance with ISO 9513 (2012) and ASTM E83 (2016). Sandpaper was attached at two edges of the specimens to increase the friction/grip between the specimens and the collet. After tensile tests, images of the tested composite specimens (camera) were taken to present the different modes of fracture. In addition, tensile tests of the neat epoxy plates were performed according to ASTM D638 (2014) standard. Epoxy plates (~3 mm thickness) were cut based on the Type II (dog-bone) specimen.

2.2.1 Flexural testing

Flexural properties of the composites and the neat epoxy resin plates were determined using a four-point bending configuration according to ASTM D7264 (2007). The tests were carried out by using a universal testing machine Zwick/Roell, model Z010, with a maximum load capacity of 10 kN. The calibration and verification of the measuring system load cell, was based on ISO 7500-1:2015 and ASTM E4-2016 standards. The specimens' thicknesses were between 3 and 4 mm following a span-to-thickness ratio of 32:1, the standard specimen width was 13 mm and the specimen length was about 20% longer than the support span. The diameter of the loading nose and supports was 6 mm. A crosshead speed of 1 mm/min was applied at the compressive face and a linear variable differential transformer transducer (RDP-LVDT) was fitted to measure the absolute linear displacement (position). The flexure strength and modulus were determined by loading 5 or more specimens to failure for each test-case; composites and neat epoxy resin.

2.2.2 Interlaminar shear strength

The interlaminar shear strength (ILSS) of carbon fibres/epoxy composites was determined by a short beam shear test, on a universal testing machine Zwick/Roell, model Z010, using a three-point short beam bending test method according to ASTM D2344 (2006). The load cell capacity of the measuring system was 10 kN. The support span was altered for each coupon set to maintain a thickness-to-span ratio of 4.0 according to the standard. In displacement control, the loading-nose travelled at a rate of 1 mm/min and the absolute linear displacement was measured a fitted RDP-LVDT.

All of the mechanical tests (summarised in Table 1) were performed in controlled laboratory atmospheric conditions i.e. room temperature at 22± 0.5 °C and relative humidity 45± 5%.

Table 1

Summary of all the mechanical tests performed to characterise the CFRPs and the neat epoxy plates.

Test-Loading	**Material**	**Method**	**Strain measurement**	**No of coupons**
Tensile 0º	CF/Epoxy	BS EN 2561-1995	Strain Gauge (both sides)	84
Flexural 90º	CF/Epoxy	ASTM D7264-2007	Transducers (LVDT)	30
ILSS	CF/Epoxy	ASTM D2344-2006	Transducers (LVDT)	40
Tensile	Epoxy-type II	ASTM D638-2014	Strain Gauge (both sides)	10
Flexural	Epoxy	ASTM D7264-2007	Transducers (LVDT)	7
Acid digestion	CF/Epoxy	ASTM D3171-2009	–	60

2.2.3 Fourier Transform Infrared Spectroscopy (FTIR)

A mid-infrared spectroscopy technique was used to identify both qualitatively and quantitatively the different functional groups on the surface of the carbon fibres. FTIR analysis of the three T700S (TORAYCA®) carbon fibres i.e. 50C, F0E and 60E, were conducted in a FTIR-8800 spectrophotometer from Shimadzu Corp., using the attenuated total reflection

(ATR) method. The crystal-prism ATR material used was diamond. Force was applied to the sample, pushing it onto the diamond surface and the IR spectrum was collected. Spectra of the fibre's surface were obtained in an optical range of 400 – 4000 cm^{-1} with 20 scans and 2 cm^{-1} of resolution. Note that carbon (black) displays absorption over the entire region from 4000 to 400 cm^{-1}. However, when using the ATR technique, the effect of carbon becomes greater with deeper light penetration at the long wavelength (low wavenumber) end. This results in a spectrum where the baseline descends at the right end. The baselines of the obtained spectra were corrected, smoothed and analysed with the SpectraGryph spectroscopy software.

2.2.5 Scanning electron microscopy (SEM)

The surface topography of the three different types of Toray fibres (50C, F0E and 60E) was examined by a Hitachi S-4700 field emission scanning electron microscope (FE-SEM) with acceleration voltage of 5 kV. In addition, the fracture morphology of the composites were observed using the scanning electron microscope with different magnifications. The non-conductive samples of CF/epoxy composites were sputter-coated with gold for a period of 5-8 minutes reaching a thickness of approximately 100Å thus improving electrical conductivity of the samples before SEM examination.

2.2.6 Dynamic Mechanical Thermal Analysis (DMTA)

The Dynamic Mechanical Thermal Analyser used for the characterization of the neat epoxy matrix and the composites was a Tritec 2000 DMA manufactured by Triton Technology, Ltd. (UK). Samples were placed in the DMTA instrument and oscillated at a frequency of 1 Hz in a single cantilever-bending configuration based on the AITM1-0003 (2010) standard. Tests were carried out at a heating rate of 5°C/min from 25 to 185°C, 0.03 mm maximum displacement and using a specimen with dimensions of around 35 × 10 × 3 mm. Note that all DMTA specimens were dried for over 48 hours at 70°C before performing the tests. Tg temperatures from DMTA tests were obtained from the onset of the change in the slope of the storage modulus (E') curve; Tg_{onset} and the maximum point of the tan δ curve; $Tg_{tan\delta}$. More specifically, Tg_{onset} was determined to be the intersection of two slopes from the E' curve where the first slope was selected at a temperature before the modulus drop step and the second slope was selected at the temperature indicating the middle point of the modulus drop.

2.2.7 Microscopic observation

The fibre distribution within the CF/epoxy composites was extensively analysed using optical microscopy. Several specimens with dimensions of 30 x 20 mm (length × width) were obtained by cutting from different locations of each of the CFRP panels, using a surface grinder. Composite samples were embedded into an epoxy resin (Epoxicure from Buehler, UK) and cured for 8 hours at room temperature. The edge of each of these specimens was polished using a grinder and polisher. Initially, three sandpapers with varying grit sizes were used (P320, P1000 and P2500) followed by diamond based dispersions; 3 µm and 1µm. The samples were examined under an optical microscope from MEIJI TECHNO CO., LTD., fitted with a camera (Motic Moticam 2300), to determine the general consolidation quality of the laminates. In addition, images taken in optical microscopy were post-processed by using the ImageJ 1.50i software and the fibre orientation on a polished surface part of the cross section of the laminates (approximately 8000 fibres), was optically characterised [36–38]. A micrograph depicting a cross sectional view of the composite can be seen in Fig. 2. Each micro-section image contained typically ~200 fully visible fibres. Functions in ImageJ software were employed to get binary photos (back/white) in order to get clear boundary of the recorded images. Additional options in ImageJ software such as "threshold", "watershed", and "remove outlier" were employed to enhance the quality of the micrographs upon the measurements. The diameter of the i_{th} carbon fibre (in pixels) was computed in ImageJ software and recorded as $D_{i,\max}$ (maximum diameter of the circular area) and $D_{i,\min}$ (minimum diameter of the circular area) values. Similarly, the fibre volume fraction (FVF) and approximately the void content of the whole cross section of CF/epoxy laminates were estimated. The FVF for the prepared laminate was measured as described above and then functions in ImageJ software; "threshold" and "fraction area", were utilized to calculate the area ratio as follows:

$$\text{Fibre Area ratio} = \left(\frac{\sum fiber\ cross\ section\ area}{total\ cross\ section\ area}\right) \qquad (1)$$

Similarly, the void content of the prepared laminates was measured by post-processing the micrographs with ImageJ software (following the aforementioned steps) and it was calculated based on the following equation:

$$\text{Void} = \left(\frac{\sum void\ cross\ section\ area}{total\ cross\ section\ area}\right) \qquad (2)$$

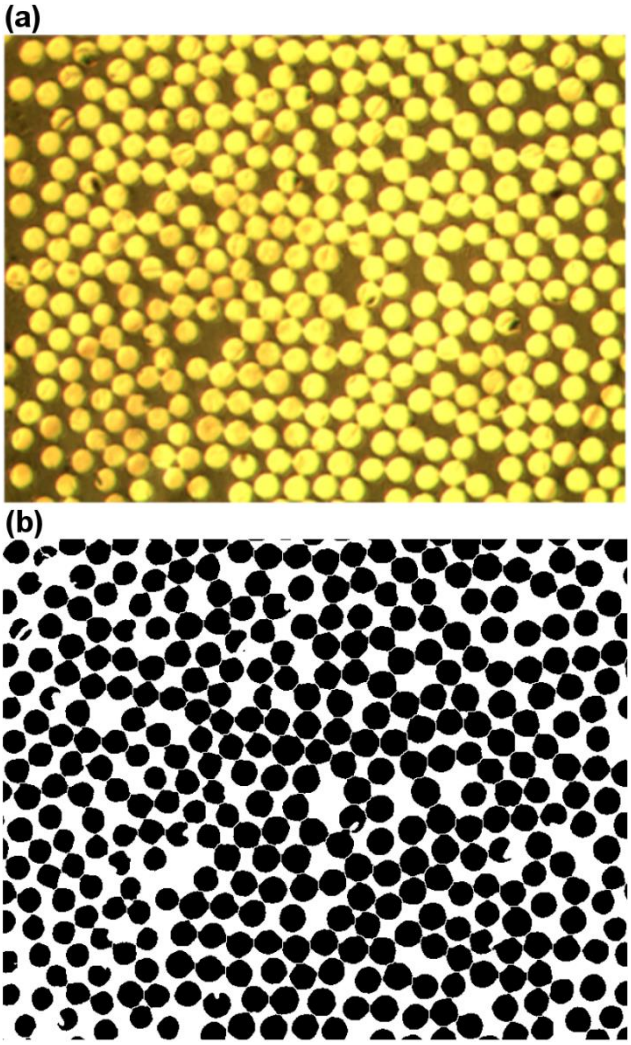

Fig. 2. (a) Typical micrograph cross section of the carbon fibre (yellow) epoxy (brown) composites and (b) obtained binary image to analyse fibre orientation, FVF and void content.

3. Results and discussion

3.1 Surface chemical properties

FTIR analysis of the T700S -50C, -F0E and -60E fibre surfaces was carried out and the obtained transmittance spectra are presented in Fig. 3. A qualitative identification of the different distribution (chemical composition) of the functional groups on the three fibres' surfaces was allowed by employing this method. Bands from 3650-3200 cm^{-1} were attributed to the stretching of hydroxyl groups (ROH) with a strong peak at 3643 cm^{-1} for all fibre types. The vibrations N−H from 3500 to 2300 cm^{-1} showed clear adsorption differences between the used fibre types [39]. Higher amount of N groups can elevate the cross-linking density in epoxy

resin systems as a result of their high functionality as reported by Packham *et al*. [40]. All fibres showed similar peaks at the positions of 2164 cm^{-1} and 2114 cm^{-1}, which were attributed to the presence of (RNH_3) azides (which can be reduced to primary amines, RNH_2) and (RC≡CR') alkyne functional groups, respectively. Since amine compounds are well-known hardeners, they are recognised as important curing-reactant agents for epoxy resin systems. The peaks at 1713, 1711 and 1709 cm^{-1} for 50C, F0E and 60E, respectively, were attributed to the vibrations of carboxylic acid (RCOOH) ketone units, a common complex mixture of oxygenated species contained on the surface of fibres [41,42]. The bands which can be ascribed to stretching of alkyne ($R_2C{=}CR_2$) functional groups vibrations occurred at 2114, 2011 and 2109 cm^{-1}, respectively, for the three fibre cases. In addition, aromatic nitro compounds (RNO_2) at 1503 cm^{-1} and 1504 cm^{-1} [43], were revealed, as displayed in Fig. 3. Note that these groups have active hydrogen which is able to open epoxy rings and contribute to the cross-linking mechanism [40]. The vibrations at the positions of 1244 – 1246 cm^{-1}, for all three fibres, and additional bands at 905 cm^{-1}, 930 cm^{-1} and 931, respectively, corresponded to stretching vibrations of epoxy compounds (RCOOR') [23,42,44–46]. The 50C fibre type i.e. highest amount of sizing agent (1%) of the 3 materials considered, showed a further peak at 830 cm^{-1} which was attributed to stretching C-O-C of oxirane group. The wave numbers at positions of 621 cm^{-1}, 622 cm^{-1} and 611 cm^{-1} for 50C, F0E and 60E, respectively, were attributed to the ($R_2C{=}CR_2$) alkyne bending groups. The FTIR analysis provided evidence that the three types of sizing agents coated on the fibres surface were epoxy type, in agreement with previous studies [21,23,42,44,45]. It is worthwhile noting that the transmittance differences observed in the obtained IR spectra connected with the slightly different chemical distribution of the functional groups on the surface of the fibre may result in a dissimilar interfacial bonding between the fibre and the matrix. Thus, these bonding variations can significantly alter and affect the final mechanical behaviour of the examined composites.

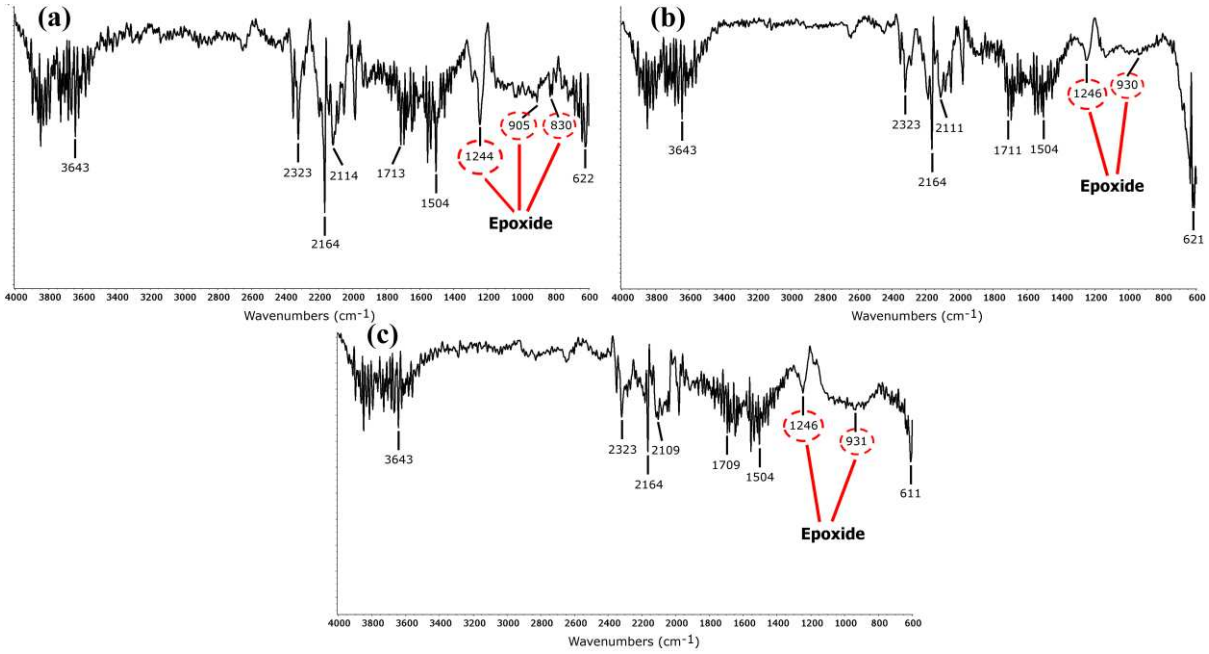

Fig. 3. FTIR spectra for T700S (a) 50C, (b) F0E and (c) 60E carbon fibre types.

3.2 Carbon fibre surface topography

Fig 4 shows SEM images of the three different carbon fibre surfaces; 50C, F0E and 60E, with the various concentrations of the sizing agent; 1%, 0.7% and 0.3%, respectively. Differences in the fibre surface topography i.e. roughness, can be observed among the three type of fibres. It is clear that the surface morphology changed when a different amount (and type) of sizing treatment was applied. In the case of the 50C fibres treated with 1% of sizing agent, some bumps (and lumps) of the aggregated polymeric sizing can be observed, Fig. 4(a). Regions with the agglomeration of the sizing agent may form defects on the surface on the carbon fibre and promote non-uniform interface interactions between the matrix and the fibres while influencing the adhesion strength of the composite. Fig. 4(b) presents a micrograph of F0E carbon fibres, indicating that there were a number of longitudinal streaks parallel to the fibre axis, originating from the manufacturing process. The surface of 60E carbon fibres was clean and smooth after being treated with a smaller amount of the sizing agent; 0.3%, Fig. 4(c). It is worthwhile noting that the longitudinal streaks observed on the F0E sized fibres became shallower as the sizing agent was increased to the 50C fibre cases, resulting in a smoother fibre surface. An increase of the fibres' surface roughness could enhance the mechanical interlocking phenomena [47]. Therefore, the surface of 50C fibres, with the highest amount of sizing agent, was related to a negative effect on mechanical interlocking but with an enhancement of

chemical interlocking. On the other hand, the 60E fibre interface clearly promoted mechanical interlocking, while the F0E may be associated to an intermediate behaviour in term of physicochemical interactions with the matrix.

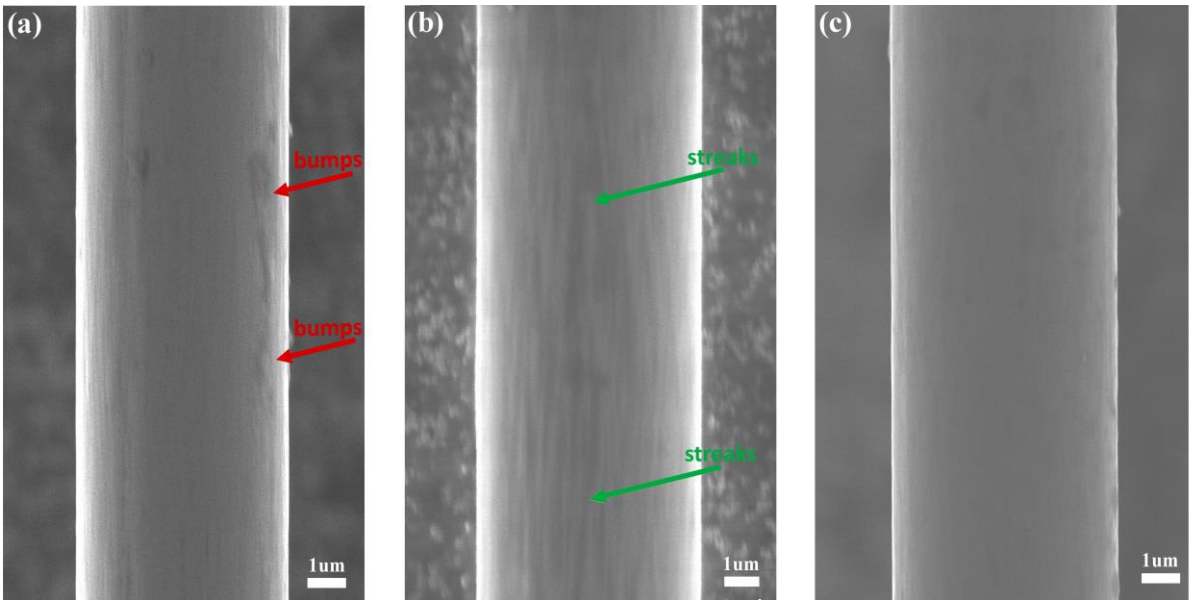

Fig. 4. SEM images of carbon fibre surface; (a) 50C, (b) F0E and (c) 60E, with the three different concentrations (and types) of sizing agents; 1%, 0.7% and 0.3%, respectively.

3.3 Fibre orientation and volume fraction

The fibre orientation (the circularity of the measured fibres) of the ith carbon fibre was calculated from the ratio ($D_{i,total} = D_{i,\min} / D_{i,\max}$) of the $D_{i,\min}$ and $D_{i,\max}$ values, minimum and maximum diameters of each visible fibre, respectively, as displayed in Fig. 2. For each fibre type (50C, F0E and 60E) of the prepared composites i.e. tension and no-tension cases, more than 9000 fibres were measured ($n > 9000$) based on the following equation:

$$f = \frac{\sum_{i=1}^{n} D_{i,total}}{n} \qquad (3)$$

where f is the direction parameter and n is number of all carbon fibre measured from the micrographs of the composites. Note that the total number of the tested visible fibres was acquired from three different laminates for each fibre type and tension/no-tension cases, respectively. The results from the overall calculations of the fibre orientation, under tension conditions, showed that $f_{50C,tension}$, $f_{F0E,tension}$ and $f_{60E,tension}$ were 0.95, 0.92 and 0.89, respectively. Additionally, for the no-tension composites cases, the unidirectional parameters; $f_{50C,no\ tension}$, $f_{F0E,no\ tension}$ and $f_{60E,no\ tension}$ were found to be 0.86, 0.88 and 0.87,

respectively (all results shown in Fig. 5). Both families of tested CFRPs (tension and no-tension) could be considered approximately unidirectional in orientation but clearly with a different degree of fibre straightness for each composite case. It is clear from Fig. 5 that the laminates manufactured under fibre tension conditions exhibit a higher degree of orientation than those manufactured without applied fibre tension. The amount of sizing agent on the fibres surface also affected the degree of fibre straightness both in tension and no-tension conditions. Additionally, the propagation of error (uncertainty) was estimated by combining individual auxiliary measurements including the cutting and grinding-polishing processes as well as the optical measurements. The error related to the cutting process was estimated by measuring the width (thickness) of each specimen that was extracted perpendicularly and it was found to be less than 1%. Since the grinding-polishing processes were automated, the only error was taken in account was the accuracy of the device during the process with an uncertainty of 0.5% (provided from the suppliers). Furthermore, as it was mentioned above, a quantitative approximation of the degree of fibre straightness for each CFRP was performed by examining more than 9000 fibres for each case from the micrographs. Thus, the (total) error propagation for each composite case was calculated and the propagation of error was represented by the error bars in Fig 5.

Table 2 compares results obtained from the fibre volume fraction and void content (volume) calculations by applying optical characterization techniques and the acid digestion method (ASTM D3171). Fibre volume fractions (FVF) calculations for all the different composites, under tension and no-tension conditions, were based on the cross-section ratio between the fibres and the matrix by using ImageJ software in comparison to the acid digestion method. Correspondingly, the void content of the composites was evaluated by employing both techniques. The results in Table 2 showed that the two applied methods of calculating the FVF and the void content revealed roughly similar values with an average FVF of ~59% and a void content of ≈1%, for all composite cases examined. Note that optical analysis of the micrographs was performed on 5 specimens for each fibre type and tensioning conditions (over 10 images for each specimen type) while experimental measurements of reinforcement or matrix FVF and void contents were conducted for all the tested laminates, with 3 measurements for each UD composite case. Fig. 6 presents typical microscopy images taken at the cross section of the composites. The fibre/matrix distribution and absence of voids, as well as the boundaries between the plies can be seen clearly in Fig. 6. The brighter (yellow) areas depict the fibres while the darker (brown) ones related to resin-rich areas. More specifically, the micrographs in

Fig. 6 (a) and (b) present fibres at 0° orientation whereas in Fig. 6(c) the fibres are orientated at 90°. It is worth mentioning that all the cases revealed the same features i.e. absence of voids and excellent consolidation, Fig. 6.

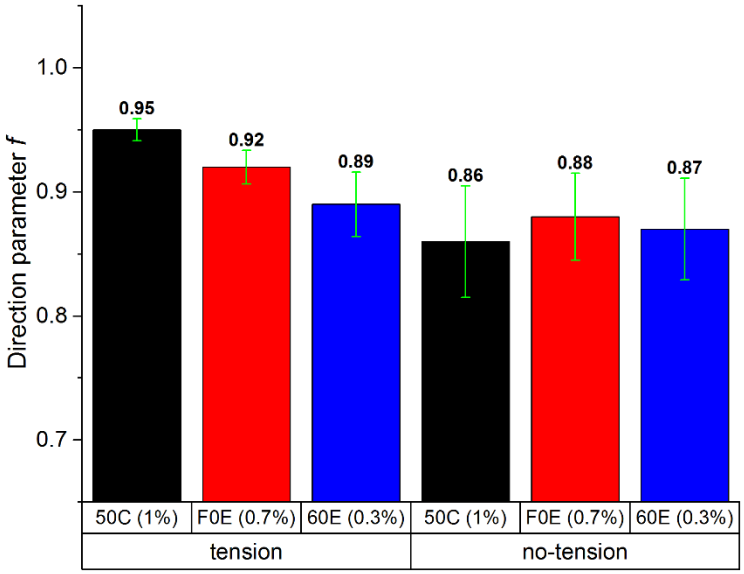

Fig. 5. Direction parameter f, as a function of the three different fibre types and tension/no-tension conditions. Error bars depict the (total) propagation of error for each composite case.

Table 2

Fibre volume fraction (FVF) measurements, standard deviation (SD), standard error of mean (SE) and void content volume related to the two different applied methods, for all the composite cases.

Method / **Composites**	**Acid digestion**					**Optical measurement**				
	FVF (%)	SD	SE	Void content (%)	SD	*FVF* (%)	SD	SE	Void content (%)	SD
50C CF/epoxy	59.1	4.0	1.5	0.85	0.4	59.4	4.8	1.3	1.05	0.2
F0E CF/epoxy	58.5	2.8	1.1	1.15	0.3	57.8	2.6	0.8	0.85	0.3
60E CF/epoxy	57.4	2.6	1.2	0.75	0.5	58.5	2.8	1.1	1.1	0.3

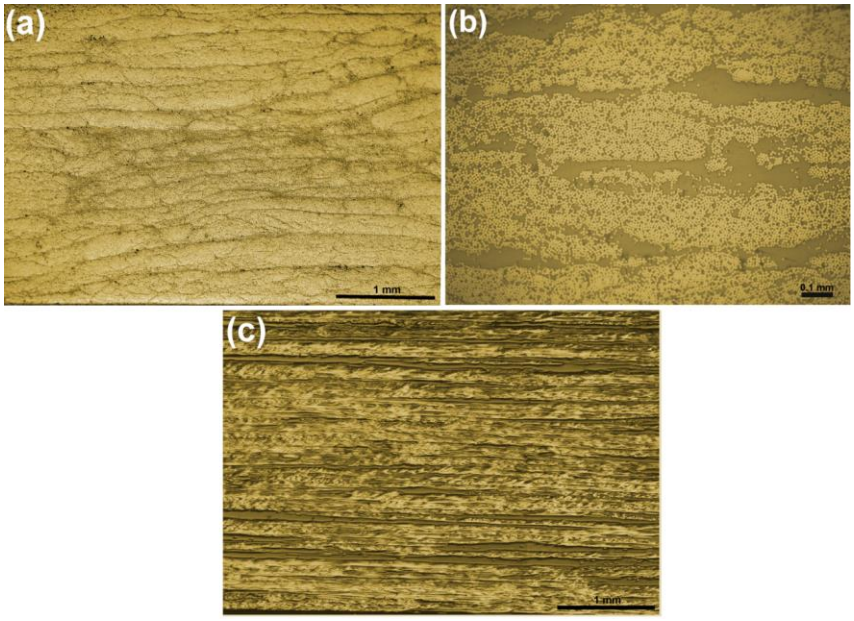

Fig. 6. Typical cross section micrographs at 0^o (a), (b) and 90^o (c) fibre orientation, respectively.

3.4 Tensile Results

The effect of varying fibre straightness, in combination with the different surface chemistry of the three carbon fibre types, on the tensile performance of CFRPs was examined. Results of the tensile tests for the six composites cases (similar FVFs) are displayed in Fig. 7. 0° tensile strength values of the UD composites reinforced with 50C fibres (~2650 MPa) was higher; +11% and +13% compared to the F0E (~2350 MPa) and 60E (~2250 MPa) composite cases, under tension conditions, respectively, as seen in Fig. 7(a). Similarly, the (0°) tensile modulus of the composites reinforced with the 50C fibres (~134 GPa) was slightly higher; +7% and +10%, than those of F0E (~126 GPa) and 60E (~121 GPa) laminates, respectively. Since the properties of the all the T700S fibre family are the same (Table 3), it is expected that the composites (of the same FVFs) will exhibit similar tensile behaviour.

Tensile results for the CFRPs under no-tension conditions showed that fibre straightness played a crucial role by decreasing the tensile performance of all the laminates examined. Interestingly, the tensile strength of the no-tension 50C-composite was decreased by around 25% compared to those where the fibres were maintained under tension during cure process. In addition, the tensile strength (average) values for the no-tension F0E and 60E composites were decreased by ~8% and ~7%, respectively, when compared with the respective composites cases with tensioned fibres. Similar trends in terms of tensile modulus were also revealed for the non-tensioned composites, Fig. 7(b). More specifically, (no-tension) 50C and F0E

composites' stiffness was reduced by ~14% and ~7% as compared to the laminates with tensioned fibres, respectively. However, the tensile modulus of the 60E composites was decreased by only 4% as compared to the tensioned case.

It is worth noting that the overall tensile performance of all the composites was enhanced when tension was applied on the fibre-tows owing to the different unidirectional character for each fibre case (Fig. 5). The tensile modulus values of 60E laminates were almost identical in both cases, pointing out that the fibres treated with a small amount of the sizing agent (0.3%) were not affected noticeably by the tensioning apparatus. Moreover, the tensile performance (both strength and modulus) of F0E tested cases was in between the 50C (1%) and 60E (0.3%) composites owing to both intermediate unidirectional character and sizing agent concentration (0.7%). The tensile properties for the composites fabricated under tension conditions were as high as those provided by the manufacturer (TORAYCA®) corresponding to a UD carbon fibre epoxy composite (FVF ~60%) where tensile strength and tensile modulus were 2550 MPa and 135 GPa, respectively [48].

Additionally, tensile tests of the pure epoxy were performed to investigate matrix properties and as reference line for engineering design purposes. Tensile modulus (average) values of the epoxy plates (dog-bones) was measured around ~3GPa.

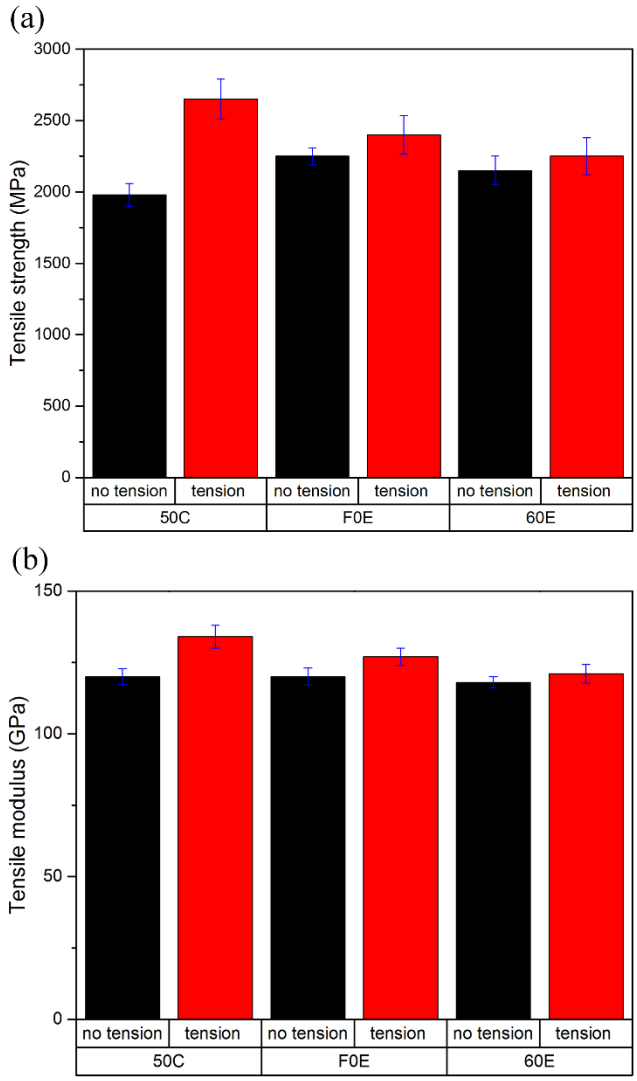

Fig. 7. Tensile results (a) tensile strength and (b) tensile modulus of the three different composites cases, under tension and no-tension conditions, respectively. The average values were calculated from ~25 tests for each composite case. Note that the obtained results were normalised at ~59% FVF for means of comparison.

Table 3 Properties of the used carbon fibres (data supplied by the respective manufacture) [48].

Property	**T700S Fibre (TORAYCA®)**		
	50C	F0E	60E
Sizing amount and type (%)	1	0.7	0.3
Tensile strength (MPa)	4900		
Tensile modulus (GPa)	230		
Filament diameter (µm)	7		

Density (g/cm^3)	1.8
Elongation at failure (%)	2.1

3.4.1 Fracture modes

Images were taken (from a camera) of the tested tensile specimens to identify the observed fracture modes. All (84) tested coupons (tension/no-tension cases) exhibited a splitting fracture mode, as presented in Fig. 8. More specifically, the majority of the tensioned composites fractured in an explosive splitting mode (~94% out of 48 tests from 6 laminates) which exhibited broom-like heads, Fig. 8(a), whereas the rest of the tested specimens (6%) fractured in long-splitting mode, Fig. 8(b). In contrast, most of the tested specimens without tension (~87% out of 36 tests from 6 laminates) fractured in long-splitting mode, and the rest of these specimens failed in an explosive manner (~13%). Fig 8(c) summarises the results obtained from the statistical analysis related to the two different fracture modes observed for the examined CFRPs. Composites with a long-splitting mode of fracture were characterised by smoother fracture surfaces compared to those which exhibited the explosive splitting mode. The fracture morphology of the failed specimens indicated that the fracture lines ran predominately along the fibre direction. The two different fracture modes observed were influenced by the varying unidirectional character of the composite and the reinforcement property i.e. the sizing amount, thus the different interfacial bonding strength between the fibre and matrix. Furthermore, it was seen that composites moulded under no-tension conditions facilitated more crack propagation, resulting in a more rapid total failure of the composite which followed by a decrease in the tensile strength of the overall laminate, as seen in Fig. 7(a). The latter can be related to the fibre misalignment for these cases, which promoted non-uniform and weaker interface performance between fibre/matrix. 50C composite (under tension) showed a better load transfer from the fibres to matrix compared to the F0E and 60E cases owing to the higher elastic behaviour which was characterised mainly by the explosive splitting failure. In our cases, the interface between the fibre/matrix played an important role in the final breakage performance. For the tensioned composite, characterised by stronger interfaces due to the higher orientation parameter, cracks propagated along the matrix while the inconsistent interfacial bonding of the no-tension composites, owing to lower fibre straightness, resulted also in an interfacial fracture where cracks propagated along the CF/epoxy interfaces.

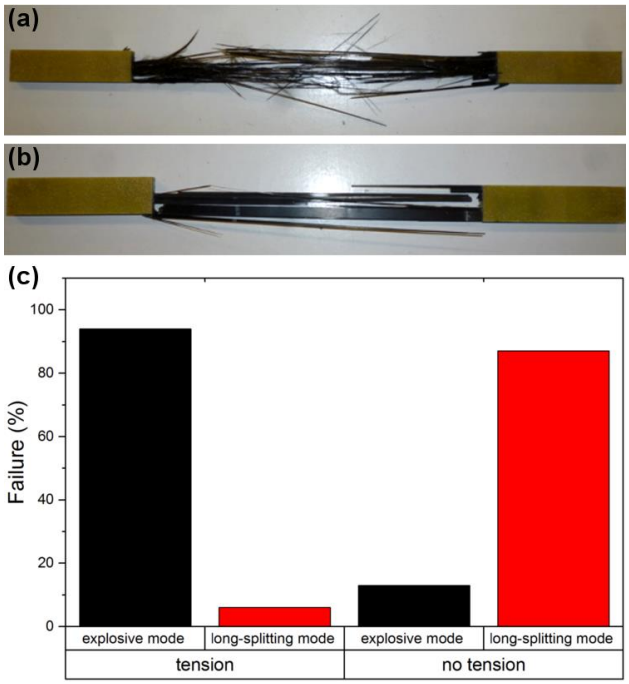

Fig. 8. Typical fracture images after the (0°) tensile tests for the CFRPs. Note that the images correspond to the splitting fracture mode where (a) is the explosive splitting and (b) the long-splitting mode. (c) Statistical analysis for the two fracture modes.

3.5 Micromechanics

The Young's modulus (E_c) of a composite material is anisotropic i.e. varies in direction, in contrast to the conventional structural engineering materials (such as steel) which are isotropic. The theoretical E_c can be estimated using the well-established Rule of Mixtures as follows [49]:

$$E_c = \kappa\eta_d\eta_I\eta_o V_f E_f + V_m E_m \qquad (4)$$

where κ is the fibre area correction factor (set at unity for circular cross-section fibres), η_d is the fibre diameter distribution factor (set at unity for man-made fibres), η_I is the interface factor, η_o is the fibre orientation distribution factor. Moreover, V_f and E_f are the fibre volume faction and Young's modulus of the fibre (see Table 3), respectively, while V_m and E_m are the matrix volume fraction ($1 - V_f - V_V$) and Young's modulus of the matrix, respectively. Note that V_V is the void volume fraction and, in our cases, was calculated around 1% (see Table 3) hence it can be neglected. The calculations of the carbon fibre orientation distribution through the direction parameter f (Figure 5) for all the CFRPs revealed an average of ~0.90. Thus, to simply the calculation, the carbon fibre orientation was approximately unidirectional oriented

and the η_o can be considered as unity. Based on the aforementioned, Table 4 presents the calculated theoretical values of both the E_c and η_I for the three different composite cases. Even an estimation of the interface factor for the three CFRP cases was performed, it was revealed that the interface bonding of 50C case seems to be the highest, then F0E and 60E cases followed. The latter is consistent with the different amounts of the sizing agent on the fibre surfaces which in turn could drastically influence the interface property in the composite.

Table 4

Micromechanics predictions for the CFRPs.

CFRP tensioned	Modulus (GPa)						η_I
	CF	V_f	Matrix	V_m	Theoretical	Tested	
50C	230	59.2	3	40.8	136.9	133.5	0.97
F0E	230	58.1	3	41.9	134.8	127.2	0.94
60E	230	58.0	3	42	134.6	121.3	0.90

3.6 Flexural properties

Transverse flexural results for all composites cases, under tension, as well as for the pure (powder) epoxy plates are plotted in Fig. 9. It can be seen that the obtained flexural strengths for the 50C (~114 MPa) and 60E (~105 MPa) cases were significantly higher; ~34% and ~28%, than those of the F0E (~76 MPa) composites, Fig. 9(a). The flexure strength results of the unreinforced epoxy specimens were not plotted as the flexure tests were optimised for testing composites (ASTM D7264) and the epoxy plates were too elastic, hence continuing to bend and reaching the limit of the testing machine. The transverse flexural test of a UD composite can be used as a method for evaluating fibre-matrix interfacial bond strength performance. Therefore, in our cases, the 50C and 60E composites exhibited better (stronger) interface bonding and resulted in higher flexural properties. Considering that the same matrix (epoxy) was used for both composites, the difference between the flexural behaviour was connected with the amount (and type) of the sizing agent and thus fibre straightness ($f_{50C,tension} \approx 0.95 > f_{F0E,tension} \approx 0.92 > f_{60E,tension} \approx 0.89$). Similarly to the tensile tests, the composites' flexural performance was affected by the unidirectional character altering the interphase interactions and the fibre-fibre interactions between each tow and ply of the composite.

Fig. 9(b) shows the results obtained for the flexural modulus of the three composites. It is clear that the trend observed for the flexural modulus (average) values of the three composites; 50C (~8.2 GPa) > F0E (~7.5 GPa) > 60E (~7.2 GPa), can be related to the different amount of the sizing on the fibre surface and in turn the varying fibre straightness (but almost UD) which altered the fibre-fibre interactions and resulted in a different crack initiation and propagation mechanism. Since the modulus in the transverse flexure tests is dominated by the matrix in the laminate; the increase in the modulus that was observed in our composites was due to the reinforcement effect of carbon fibres, which prevented early sliding of the polymer phase [49].

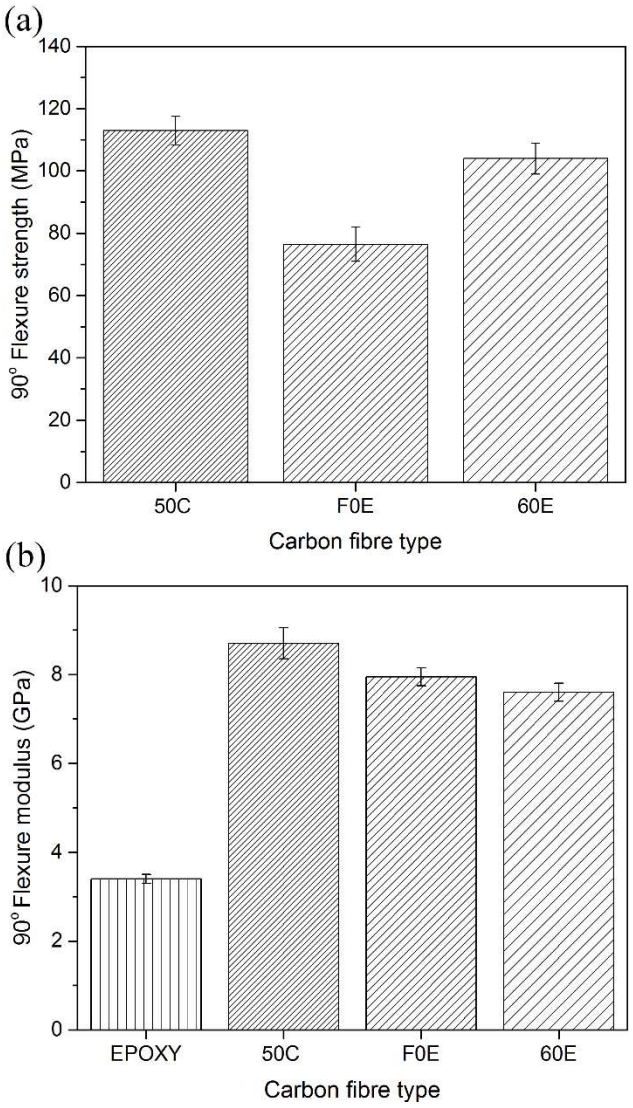

Fig. 9. Transverse flexural results (a) strength and (b) modulus, obtained for T700S family composites, under tensioning conditions, as well as for the neat (powder) epoxy blocks. The flexural values are

averages from 15 tests for each case. Note that the obtained results were normalised at ~59% FVF for means of comparison.

3.7 Fracture topography of the composites

Mechanical properties of composites are linked to their structure and the macroscopically observed failure modes are closely connected with the microscopic failure mechanisms. Toward a further understanding of the mechanical performance for the three composites cases, the fractured surface of the samples after transverse flexural tests; four-point bending mode, was comparatively examined under scanning electron microscopy. Typical SEM images of the fracture surfaces for the 50C, F0E and 60E composites tested in flexure are shown in Fig. 10 (a) – (f). The fracture surface morphology of the three different cases was seen to be different hence indicating that a dissimilar crack propagation mechanism occurred. Since the same matrix; (powder) epoxy, was used for all the composites, the difference between fibre adhesion strength was associated with the carbon fibre surface properties (see Table 3) and the fibre straightness (see also Fig. 5). In all cases, ductile deformation of the matrix was observed on the fracture surfaces of the specimens which was characterised by a stable crack propagation demonstrating strong interfacial adhesion between fibre and matrix. At higher magnification, Fig. 10 (b), (d) and (f), it can be clearly seen that fibre surfaces were covered by large amounts of epoxy and some visible epoxy agglomerates appeared. The latter was typical of a cohesive failure of the matrix under flexural forces, confirming a good interface bonding in all fibre composites cases examined. In addition, no signs of delamination between the fibres and the matrix were observed, implying that complete epoxy wet-out has occurred. It is worthwhile noting that the fracture morphology of the F0E composite case was characterised by the formation of hackles, Fig. 10(d), demonstrating matrix shear failure due to lower cohesive strength i.e. lower toughness, resulted in a characteristic weaker flexural strength of the laminates, as displayed in Fig. 9(a). Note that an excellent fibre-matrix distribution was revealed owing to the high UD character of all the composites (under tension conditions).

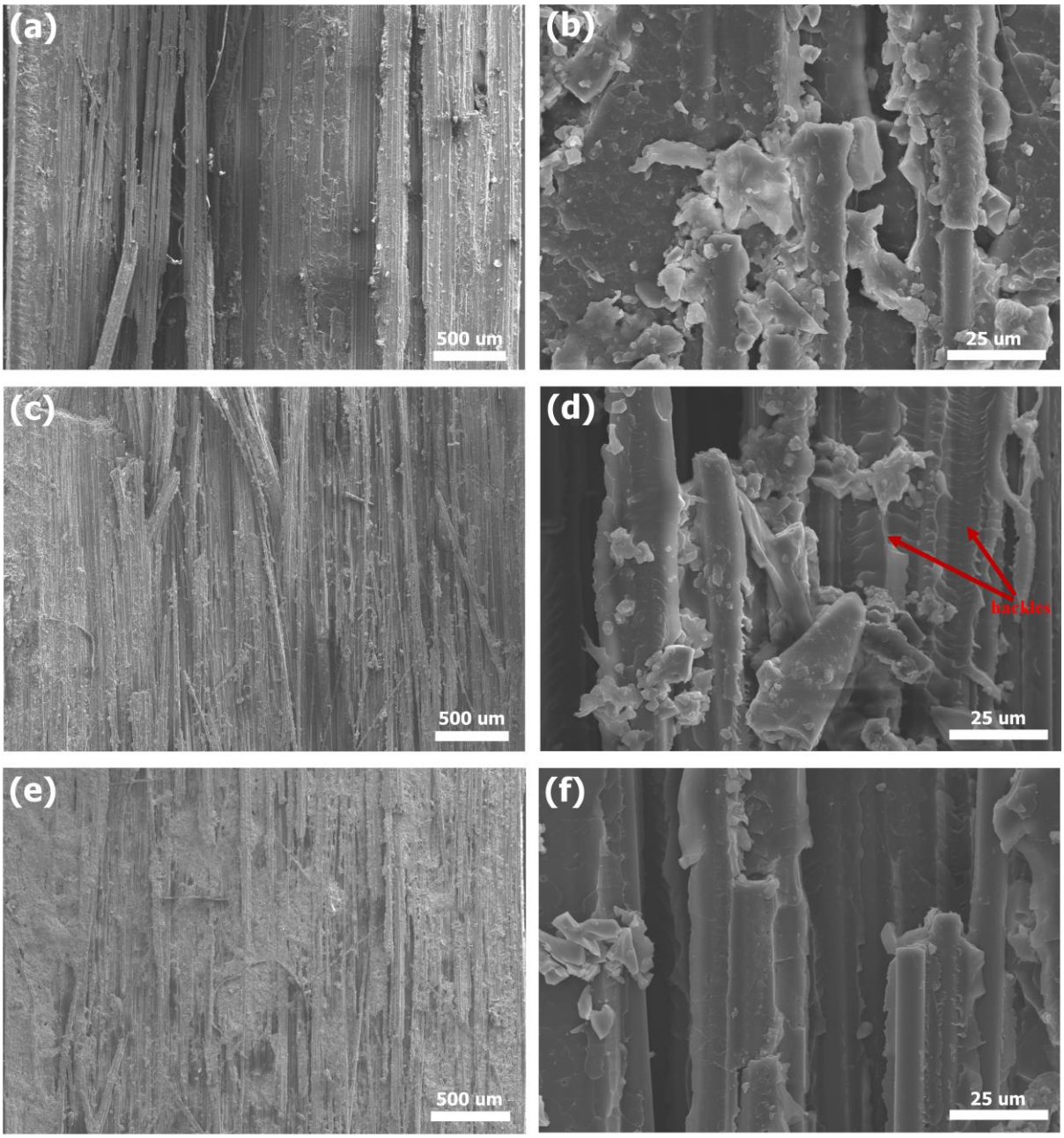

Fig. 10. SEM micrographs on the fracture surface of the three different (90°) flexure composite cases (under tension); 50C (a) and (b), F0E (c) and (d) and 60E (e) and (f) fibres types.

3.8 ILSS

The short beam method is a common test method used to estimate the interlaminar shear strength between the fibre and matrix. Interfacial adhesion between fibres and matrix has a strong influence on the interlaminar performance of composites [19,45,50]. In addition, the sizing layer on the fibres' surface significantly affects the final mechanical properties of the composite [23,47]. The effect of the three different reinforcements on the interlaminar

properties of CF/epoxy composites has been examined, and the results are shown in Fig. 11. The interlaminar shear strength of the 60E tensioned composites was slightly higher than that of the 50C and F0E tensioned cases. The observed behaviour can be explained by the different physicochemical interactions between the fibre surface and the matrix of the three composites owing to the different sizing agent property (and amount) as well as the varying direction parameter (Fig. 5). The strong interfacial bonding between the fibre and the plies was also revealed from the ILSS tests connected with the measured low void content for all examined composites. However, the slightly higher interlaminar performance of the 60E composite could be a result of the increased structural integrity of the material through better mechanical interlocking (lower amount of sizing agent) than those of the 50C and F0E cases, which resulted in promoting the applied stress transfer from the matrix to the fibres. Moreover, the slightly lower fibre straightness revealed for the 60E tensioned cases than those of 50C and F0E could enhance the interlaminar shear strength as a result of the fibre-fibre interactions between the plies.

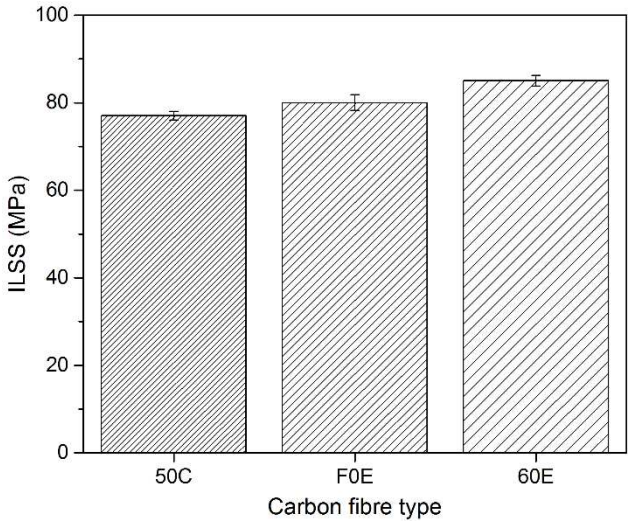

Fig. 11. ILSS results of the three carbon fibres epoxy composite cases, processed under tensioned conditions.

3.9 Dynamic mechanical analyses

The characterisation of dynamic (thermomechanical) properties in composites via DMTA are of prime importance in understanding the structure/properties relationships of composites when assessed over a range of temperatures and frequencies [51].

A comparison of dynamic mechanical properties of the 50C, F0E and 60E tensioned composites as well as the neat epoxy is given in Fig. 12. It can be seen that the 50C composite presents the highest E' modulus, after the 60E and then the F0E composite. Tg_{onset} is defined as the first inflection point, or the onset of the drop in E' modulus and it is associated with the increase of polymer chain mobility. However, in all cases, the storage modulus drop occurs at similar Tg_{onset} temperatures, as displayed in Table 5. In composites, a higher E' modulus is related to better interfacial adhesion strength between fibre and matrix [21]. Regarding the damping behaviour in our tensioned composites, a lower energy dissipation on the interface i.e. lower tan δ peak height and higher $Tg_{tan\delta}$ value, is associated with stronger interface bonding between matrix/fibre [52]. The latter can be explained by more restricted movements of the polymer chains and effective stress transfer in the material. Therefore, in our cases, 50C and F0E composites are characterised by a relatively similar interfacial bonding but better than that of the 60E case (see also Table 5). In addition, for higher chain segments movement, greater the area under the tan δ peak and weaker interfacial adhesion strength is predicted. In this case, 50C and F0E composites have roughly the same area whereas the 60E is characterised by a larger one.

The viscous response (loss modulus) of the composites cases and the neat epoxy is presented in Fig. 12(b). Since the E''curve is a measure of dissipated energy as heat per cycle, the height of the curve is attributed to the relaxation process. In turn, a higher E'' peak can means more energy dissipation and weaker interface bonding. This is due to the increase of the internal friction and an increase in the mobility of the polymer chains [52–54]. According to Fig. 12(b), the 60E composite shows the highest E'' value, indicating weaker bonding while the 50C and F0E composites had lower values, respectively. In the F0E case, an apparent shift in Tg toward higher temperatures was observed, indicating a segmental immobilization of the chains at the fibre surface which is attributed to good interfacial adhesion [55].

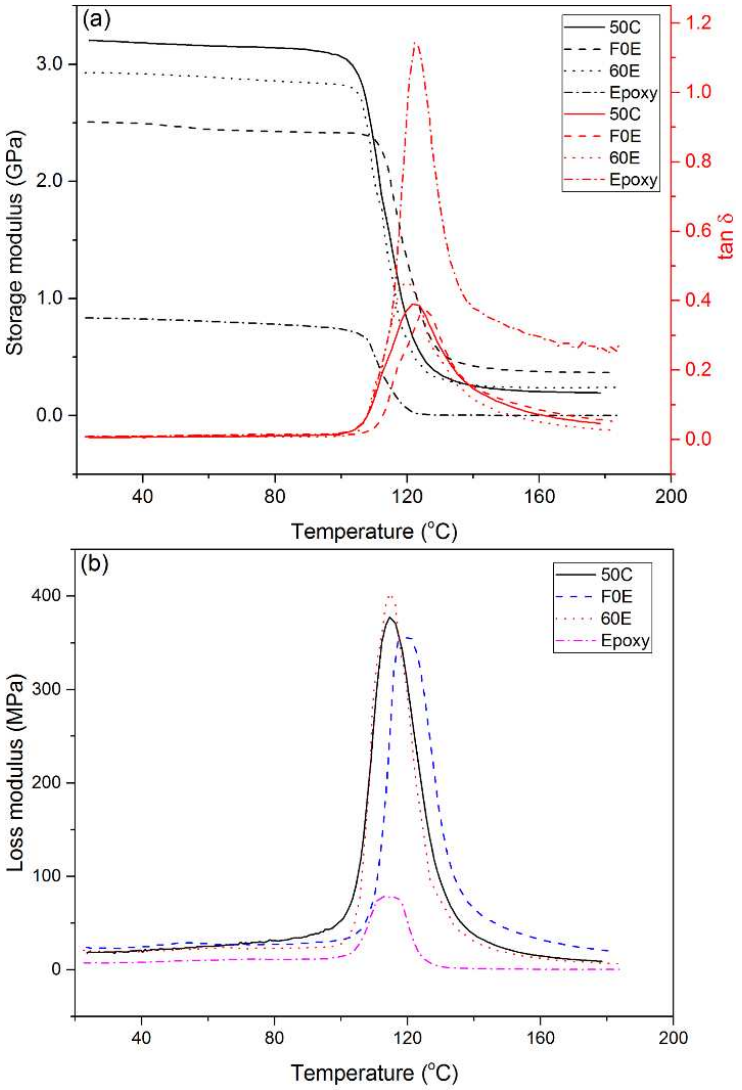

Fig. 12. Dynamic mechanical properties of the Toray family (50C, F0E, 60E) composites (UD cantilevered specimens with the fibres running transverse to the loading) and the neat epoxy case.

Table 5

The Tg_{onset} and $Tg_{tan\delta}$ values are measured at the onset of E' change and peak of the tan δ curve, respectively. Note that the Tg values obtained are averages from around 8 DMTA tests for each composite (under tensioning conditions) and neat epoxy case.

Material	**~Tg_{onset}**	**~$Tg_{tan\delta}$**
Neat epoxy	105.5°C	125.6°C
50C CF/Epoxy	105.8°C	123.8°C
F0E CF/Epoxy	109.5°C	125.2°C

60E CF/Epoxy	104.6°C	122.1°C

Toward a further understanding of the effectiveness of fibre on the moduli and the viscoelastic behaviour of the three different composite cases, a coefficient "C" was calculated and is given in the following equation [52,56,57]:

$$C = \frac{(E'_G/E'_R)_{composite}}{(E'_G/E'_R)_{epoxy}} \quad (6)$$

where E'_G and E'_R are the storage modulus values in the glassy and rubbery region, respectively. For all cases, the measured E' values at 60°C and 170°C were employed as the E'_G and E'_R, respectively. The coefficient C represents a relative measurement of the modulus drop as the temperature increases and the material passes the Tg region. Therefore, lower C values indicate higher effectiveness of the fibre on the modulus. It is important to state that the storage modulus in the glassy region is primarily ascribed to the strength of the intermolecular forces and the polymer chain packing [57,58]. The C values are obtained for the 50C, F0E and 60E composite cases, at frequencies of 1 Hz, were 0.11, 0.14 and 0.19, respectively. It can be observed that all composites cases obtained characteristic low coefficient C values, indicating strong interface bonding and effective stress transfer between the fibre and matrix attributed to the different sizings. Considering the overall viscoelastic performance of the composites obtained from DMTA tests, the 50C sizing seems to have higher interfacial bonding performance, after F0E and 60E composites, in good agreement with all the mechanical tests discussed above.

Conclusions

In this study, unidirectional CFRPs made of reinforcing carbon fibres with three types of sizings (50C, F0E and 60E) were manufactured through a novel hand lay-up process. A specially designed tensioning apparatus was developed to apply tension on the carbon fibre tows during laminate processing, targeting an improvement of fibre straightness. Physicochemical parameters such as chemical composition of sizing, fibre surface topography and volume fraction, void content and interfacial properties were measured and calculated through a range of experimental test methods including FTIR, SEM, optical techniques, 0° tensile, 90° flexural, ILSS and DMTA. Fibre orientation of the composites was examined using

optical microscopy, demonstrating that the type of reinforcement played a crucial role by increasing or decreasing the UD character of the composites according to the applied tensioning conditions. It was found that tensioned and no-tension composites could be characterised by a varying degree of fibre straightness (direction parameter, f). The latter was due to the distinct fibre-fibre interactions affected directly from the sizing amount on the carbon fibre surfaces for each CFRP case. The overall tensile performance of the tensioned composites was increased compared to those without tension. In the case of the 50C tensioned composites, a significant enhancement in tensile strength and tensile modulus was revealed of ~25% and ~14%, respectively, compared to those CFRPs without tensioned fibres. Tensioning of the fibres, during processing, had a remarkable effect on improving the unidirectional character and the (0^o) mechanical properties, where more sizing was present (50C>F0E>60E). .

Mechanical properties (flexural, ILSS) and failure behaviour (SEM) of the tensioned composites showed strong interface bonding between the epoxy and the fibres. Nevertheless, the interfacial adhesion strength of the tensioned composites was clearly associated with the surface chemistry of the carbon fibres and in turn the different direction parameters of each composite case. Experimental results from DMTA suggested that the 50C-sized composite case was characterised by a stronger interfacial bonding compared to the other cases, owing to both highest fibre straightness and amount of sizing agent (~1%). In summary, the improved unidirectional character of the CFRPs, combined with the high uniformity, good consolidation quality and interface bonding due to the use of powder epoxy delivered high-performance UD composites characterised by enhanced mechanical properties as well as higher stiffness and rigidity suitable for marine applications. Future work will focus on further examination of the mechanical and chemical performance of the composites under seawater conditions to fully understanding the effect of moisture and corrosion at the interface between the matrix and the fibres.

Acknowledgments

This work was carried out with funding from MARINCOMP, Novel Composite Materials and Processes for Marine Renewable Energy, Funded under: EU FP7-People, Industry Academia Partnerships and Pathways (IAPP), Project reference: 612531. We also acknowledge funding from POWDERBLADE, Commercialisation of Advanced Composite Material Technology: Carbon-Glass Hybrid in Powder Epoxy for Large Wind Turbine Blades, Funded under:

Horizon 2020, Fast Track to Innovation Pilot, Project reference: 730747. The authors thank Composites Testing Laboratory (Ireland), for performing a series of tests for the work.

References

[1] Shams SS, El-Hajjar RF. Overlay patch repair of scratch damage in carbon fiber/epoxy laminated composites. Compos Part A Appl Sci Manuf 2013;49:148–56. doi:10.1016/j.compositesa.2013.03.005.

[2] Tehrani M, Boroujeni AY, Hartman TB, Haugh TP, Case SW, Al-Haik MS. Mechanical characterization and impact damage assessment of a woven carbon fiber reinforced carbon nanotube–epoxy composite. Compos Sci Technol 2013;75:42–8. doi:10.1016/j.compscitech.2012.12.005.

[3] Soutis C. Carbon fiber reinforced plastics in aircraft construction. Mater Sci Eng A 2005;412:171–6. doi:10.1016/j.msea.2005.08.064.

[4] Penn L, Wang H. Epoxy resins. In: Peters ST, editor. Handb. Compos. 2nd ed., Boston, MA: Springer US; 1998, p. 48–74. doi:10.1007/978-1-4615-6389-1.

[5] Graham-Jones J, Summerscales J. Marine applications of advanced fibre-reinforced composites. Amsterdam : Elsevier Ltd.; 2016.

[6] Figliolini AM, Carlsson LA. Mechanical properties of carbon fiber/vinylester composites exposed to marine environments. Polym Compos 2014;35:1559–69. doi:10.1002/pc.22809.

[7] Brøndsted P, Lilholt H, Lystrup A. COMPOSITE MATERIALS FOR WIND POWER TURBINE BLADES. Annu Rev Mater Res 2005;35:505–38. doi:10.1146/annurev.matsci.35.100303.110641.

[8] Rafique I, Kausar A, Muhammad B. Epoxy Resin Composite Reinforced with Carbon Fiber and Inorganic Filler: Overview on Preparation and Properties. Polym Plast Technol Eng 2016;55:1653–72. doi:10.1080/03602559.2016.1163597.

[9] Guo H, Huang Y, Liu L, Shi X. Effect of epoxy coatings on carbon fibers during manufacture of carbon fiber reinforced resin matrix composites. Mater Des 2010;31:1186–90. doi:10.1016/j.matdes.2009.09.034.

[10] Paiva JMF de, Mayer S, Rezende MC. Comparison of tensile strength of different

carbon fabric reinforced epoxy composites. Mater Res 2006;9:83–90. doi:10.1590/S1516-14392006000100016.

[11] Zhang K, Gu Y, li M, Zhang Z. Effect of rapid curing process on the properties of carbon fiber/epoxy composite fabricated using vacuum assisted resin infusion molding. Mater Des 2014;54:624–31. doi:10.1016/j.matdes.2013.08.065.

[12] Meijer HEH, Govaert LE. Mechanical performance of polymer systems: The relation between structure and properties. Prog Polym Sci 2005;30:915–38. doi:10.1016/j.progpolymsci.2005.06.009.

[13] Kong J, Ning R, Tang Y. Study on modification of epoxy resins with acrylate liquid rubber containing pendant epoxy groups. J Mater Sci 2006;41:1639–41. doi:10.1007/s10853-005-1862-6.

[14] Flanagan T, Maguire J, O Brádaigh C, Mayorga P, Doyle A. Smart Affordable Composite Blades for Tidal Energy. EWTEC11, 2015.

[15] Misev T., van der Linde R. Powder coatings technology: new developments at the turn of the century. Prog Org Coatings 1998;34:160–8. doi:10.1016/S0300-9440(98)00029-0.

[16] Maguire JM, Nayak K, Ó Brádaigh CM. Characterisation of epoxy powders for processing thick-section composite structures. Mater Des 2018;139:112–21. doi:10.1016/J.MATDES.2017.10.068.

[17] Belder E., Rutten HJ., Perera D. Cure characterization of powder coatings. Prog Org Coatings 2001;42:142–9. doi:10.1016/S0300-9440(01)00149-7.

[18] Ó Brádaigh CM, Doyle A, Doyle D, Feerick PJ. Electrically-heated ceramic composite tooling for out-of-autoclave manufacturing of large composite structures. SAMPE J 2011;47:6–14.

[19] Sharma M, Gao S, Mäder E, Sharma H, Wei LY, Bijwe J. Carbon fiber surfaces and composite interphases. Compos Sci Technol 2014;102:35–50. doi:10.1016/j.compscitech.2014.07.005.

[20] Qian X, Chen L, Huang J, Wang W, Guan J. Effect of carbon fiber surface chemistry on the interfacial properties of carbon fibers/epoxy resin composites. J Reinf Plast Compos 2013;32:393–401. doi:10.1177/0731684412468369.

[21] Brocks T, Cioffi MOH, Voorwald HJC. Effect of fiber surface on flexural strength in carbon fabric reinforced epoxy composites. Appl Surf Sci 2013;274:210–6. doi:10.1016/j.apsusc.2013.03.018.

[22] Song W, Gu A, Liang G, Yuan L. Effect of the surface roughness on interfacial properties of carbon fibers reinforced epoxy resin composites. Appl Surf Sci 2011;257:4069–74. doi:10.1016/j.apsusc.2010.11.177.

[23] Dai Z, Shi F, Zhang B, Li M, Zhang Z. Effect of sizing on carbon fiber surface properties and fibers/epoxy interfacial adhesion. Appl Surf Sci 2011;257:6980–5. doi:10.1016/j.apsusc.2011.03.047.

[24] Paiva MC, Nardin M, Bernardo CA, Schultz J. Influence of thermal history on the results of fragmentation tests on high-modulus carbon-fibre/polycarbonate model composites. Compos Sci Technol 1997;57:839–43. doi:10.1016/S0266-3538(96)00173-X.

[25] Blackketter DM, Upadhyaya D, King TR, King JA. Evaluation of fiber surfaces treatment and sizing on the shear and transverse tensile strengths of carbon fiber-reinforced thermoset and thermoplastic matrix composites. Polym Compos 1993;14:430–6. doi:10.1002/pc.750140510.

[26] Reis MJ, Botelho Do Rego AM, Lopes Da Silva JD, Soares MN. An XPS study of the fibre-matrix interface using sized carbon fibres as a model. J Mater Sci 1995;30:118–26. doi:10.1007/BF00352140.

[27] Wang J, Zhou Z, Huang X, Zhang L, Hu B, Moyo S, et al. Effect of alcohol pretreatment in conjunction with atmospheric pressure plasmas on hydrophobizing ramie fiber surfaces. J Adhes Sci Technol 2013;27:1278–88. doi:10.1080/01694243.2012.738323.

[28] Charles M. Kausch, Yongsin Kim, Vernon M. Russell, Robert E. Medsker and, Thomas* RR. Surface Tension and Adsorption Properties of a Series of Bolaamphiphilic Poly(fluorooxetane)s 2003. doi:10.1021/LA034233Q.

[29] Fairuz AM, Sapuan SM, Zainudin ES, Jaafar CNA. POLYMER COMPOSITE MANUFACTURING USING A PULTRUSION PROCESS: A REVIEW. Am J Appl Sci 2014;11:1798–810. doi:10.3844/ajassp.2014.1798.1810.

[30] Fairuz AM, Sapuan SM, Zainudin ES, Jaafar CNA. Effect of filler loading on mechanical properties of pultruded kenaf fibre reinforced vinyl ester composites. J Mech Eng Sci ISSN (Print 2016;10:2289–4659. doi:10.15282/jmes.10.1.2016.16.0184.

[31] Song YS, Youn JR, Gutowski TG. Life cycle energy analysis of fiber-reinforced composites. Compos Part A Appl Sci Manuf 2009;40:1257–65. doi:10.1016/J.COMPOSITESA.2009.05.020.

[32] Chandrashekhara K, Sundararaman S, Flanigan V, Kapila S. Affordable composites using renewable materials. Mater Sci Eng A 2005;412:2–6. doi:10.1016/J.MSEA.2005.08.066.

[33] Paulsen US, Madsen HA, Kragh KA, Nielsen PH, Baran I, Hattel J, et al. DeepWind-from Idea to 5 MW Concept. Energy Procedia 2014;53:23–33. doi:10.1016/J.EGYPRO.2014.07.212.

[34] Baran I, Hattel JH, Tutum CC, Akkerman R. Pultrusion of a vertical axis wind turbine blade part-II: combining the manufacturing process simulation with a subsequent loading scenario. Int J Mater Form 2015;8:367–78. doi:10.1007/s12289-014-1178-7.

[35] Maguire J, Roy AS, Doyle D, Logan M, O Brádaigh C. Resin Characterisation for Numerical Modelling of Through-Thickness Resin Flow During OOA Processing of Thick-Section Wind or Tidal Turbine Blades. Proc. ICCM20, 2015, p. 3307–2.

[36] Rossoll A, Moser B, Mortensen A. Tensile strength of axially loaded unidirectional Nextel 610^{TM} reinforced aluminium: A case study in local load sharing between randomly distributed fibres. Compos Part A Appl Sci Manuf 2012;43:129–37. doi:10.1016/j.compositesa.2011.09.027.

[37] Ma Y, Yang Y, Sugahara T, Hamada H. A study on the failure behavior and mechanical properties of unidirectional fiber reinforced thermosetting and thermoplastic composites. Compos Part B Eng 2016;99:162–72. doi:10.1016/j.compositesb.2016.06.005.

[38] Liu H, Ogi K, Miyahara H. The fibre distribution of Al2O3/Al–Cu alloy composites. J Mater Sci 1998;33:3615–22. doi:10.1023/A:1004607413182.

[39] Donnet JB, Rebouillat S, Wang TK, Peng JCM. Carbon fibers. 3th ed. Marcel Dekker, New York; 1998.

[40] Packham DE. Handbook of adhesion. United Kingdom: John Wiley & Sons, Ltd.; 2005.

[41] Marieta C, Schulz E, Mondragon I. Characterization of interfacial behaviour in carbon-fibre/cyanate composites. Compos Sci Technol 2002;62:299–309. doi:10.1016/S0266-3538(01)00215-9.

[42] Wu Q, Li M, Gu Y, Wang S, Wang X, Zhang Z. Reaction of carbon fiber sizing and its influence on the interphase region of composites. J Appl Polym Sci 2015;132:41917. doi:10.1002/app.41917.

[43] Stuart B. Polymer analysis. John Wiley & Sons Press, Ltd.; 2002.

[44] Wu Q, Li M, Gu Y, Wang S, Yao L, Zhang Z. Effect of sizing on interfacial adhesion of commercial high strength carbon fiber-reinforced resin composites. Polym Compos 2016;37:254–61. doi:10.1002/pc.23176.

[45] Ma Q, Gu Y, Li M, Wang S, Zhang Z. Effects of surface treating methods of high-strength carbon fibers on interfacial properties of epoxy resin matrix composite. Appl Surf Sci 2016;379:199–205. doi:10.1016/j.apsusc.2016.04.075.

[46] Gonzlez M, Carlos J, Baselg J. Applications of FTIR on Epoxy Resins - Identification, Monitoring the Curing Process, Phase Separation and Water Uptake. Infrared Spectrosc. - Mater. Sci. Eng. Technol., InTech; 2012. doi:10.5772/36323.

[47] Dilsiz N, Wightman J. Surface analysis of unsized and sized carbon fibers. Carbon N Y 1999;37:1105–14. doi:10.1016/S0008-6223(98)00300-5.

[48] TORAYCA® T700S DATA SHEET 2017. http://www.toraycfa.com/pdfs/T700SDataSheet.pdf.

[49] Abot JL, Song Y, Schulz MJ, Shanov VN. Novel carbon nanotube array-reinforced laminated composite materials with higher interlaminar elastic properties. Compos Sci Technol 2008;68:2755–60. doi:10.1016/j.compscitech.2008.05.023.

[50] Zhang RL, Huang YD, Li N, Liu L, Su D. Effect of the concentration of the sizing agent on the carbon fibers surface and interface properties of its composites. J Appl Polym Sci 2012;125:425–32. doi:10.1002/app.35616.

[51] Wolfrum J, Ehrenstein GW, Avondet MA. Dynamical Mechanical Thermoanalysis of

High Performance Reinforced Materials Influences and Problems. J Therm Anal Calorim 1999;56:1147–54. doi:10.1023/A:1010109129224.

[52] Hameed N, Sreekumar PA, Francis B, Yang W, Thomas S. Morphology, dynamic mechanical and thermal studies on poly(styrene-co-acrylonitrile) modified epoxy resin/glass fibre composites. Compos Part A Appl Sci Manuf 2007;38:2422–32. doi:10.1016/j.compositesa.2007.08.009.

[53] Martínez-Hernández AL, Velasco-Santos C, de-Icaza M, Castaño VM. Dynamical–mechanical and thermal analysis of polymeric composites reinforced with keratin biofibers from chicken feathers. Compos Part B Eng 2007;38:405–10. doi:10.1016/j.compositesb.2006.06.013.

[54] Manikandan Nair K., Thomas S, Groeninckx G. Thermal and dynamic mechanical analysis of polystyrene composites reinforced with short sisal fibres. Compos Sci Technol 2001;61:2519–29. doi:10.1016/S0266-3538(01)00170-1.

[55] Joseph PV, Mathew G, Joseph K, Groeninckx G, Thomas S. Dynamic mechanical properties of short sisal fibre reinforced polypropylene composites. Compos Part A Appl Sci Manuf 2003;34:275–90. doi:10.1016/S1359-835X(02)00020-9.

[56] Chua PS. Dynamic mechanical analysis studies of the interphase. Polym Compos 1987;8:308–13. doi:10.1002/pc.750080505.

[57] Ornaghi HL, Bolner AS, Fiorio R, Zattera AJ, Amico SC. Mechanical and dynamic mechanical analysis of hybrid composites molded by resin transfer molding. J Appl Polym Sci 2010;118:887–896. doi:10.1002/app.32388.

[58] Pothan LA, Thomas S, Groeninckx G. The role of fibre/matrix interactions on the dynamic mechanical properties of chemically modified banana fibre/polyester composites. Compos Part A Appl Sci Manuf 2006;37:1260–9. doi:10.1016/j.compositesa.2005.09.001.